COMMUNICATIONS CHEMISTRY

ARTICLE

https://doi.org/10.1038/s42004-019-0121-8 OPEN

Photo-triggered phase transition of a crystal

Takuya Taniguchi [1], Hiroyasu Sato[2], Yuki Hagiwara[3], Toru Asahi[1,4] & Hideko Koshima [4]

Structural phase transitions induced by external stimuli such as temperature, pressure, electromagnetic fields, and light play crucial roles in controlling the functions of solid-state materials. Here we report a new phase transition, referred to as the photo-triggered phase transition, of a photochromic chiral salicylideneamine crystal. The crystal, which exhibits a thermal single-crystal-to-single-crystal phase transition which is reversible upon heating and cooling, transforms to the identical phase upon light irradiation at temperatures lower than the thermal transition temperature. The photo-triggered phase transition originates from the strain of *trans*-keto molecules produced by enol–keto photoisomerization owing to the small energy barrier associated with changes in the crystal structure. The photo-triggered phase is metastable and returns to the initial stable phase via back isomerization from the *trans*-keto to enol form.

[1] Department of Advanced Science and Engineering, Graduate School of Advanced Science and Engineering, Waseda University, 3-4-1 Okubo, Shinjuku-ku, Tokyo 169-8555, Japan. [2] Rigaku Corporation, Matsubara-cho 3-9-12, Akishima-shi, Tokyo 196-8666, Japan. [3] Department of Life Science and Medical Bioscience, School of Advanced Science and Engineering, Waseda University, 3-4-1 Okubo, Shinjuku-ku, Tokyo 169-8555, Japan. [4] Research Organization for Nano & Life Innovation, Waseda University, 513 Wasedatsurumaki-cho, Shinjuku-ku, Tokyo 162-0041, Japan. Correspondence and requests for materials should be addressed to H.K. (email: hkoshima@aoni.waseda.jp)

A structural phase transition is a fundamental phenomenon that changes the functions of solid-state materials. It is well known that changes in temperature and pressure cause structural phase transitions and greatly change the physical properties of the solid. For instance, ferroelectrics and ferromagnets undergo structural phase transitions at the material-specific Curie temperature, resulting in unique electrical and magnetic behaviors[1–4]. Shape memory alloys exhibit the shape recovery effect due to the martensitic transition upon heating[5,6]. Light is also an external stimulus for structural phase transitions. In photo-induced phase transitions, a new crystal phase appears by light irradiation and changes the electrical and magnetic properties rapidly[7–10]. Other external stimuli, such as electromagnetic fields and solvents, also induce structural phase transitions[11–13]. Phase transition mechanisms are widely used in memory, switch, and actuation materials[14,15]; thus, the discovery of a structural phase transition has potential for both basic science and application fields.

With respect to the function(s) associated with the phase transition, we focus on actuation behavior because mechanically responsive molecular crystals are fascinating candidates for next-generation actuators[16,17]. Structural phase transitions in molecular crystals lead to actuation such as expansion/contraction[18–20], bending[21], jumping[22,23], and locomotion[24]. In addition to the structural phase transition, photochromic reactions also lead to crystal actuation[25–29]. Although photomechanical motion is mostly limited to monotonous bending, the combination of structural phase transition and photochromic reaction can induce unique bending behavior[30].

This study reports on the photo-triggered phase transition, which differs from previous structural phase transitions. The photo-triggered phase transition was discovered in the crystal of (*S*)-*N*-3,5-*di*-*tert*-butylsalicylidene-1-(1-naphthyl)ethylamine in the enol form [enol-(*S*)-**1**], which undergoes enol–keto photoisomerization (Fig. 1). The enol-(*S*)-**1** crystal exhibits structural phase transitions among trimorphic α-, β-, and γ-phases due to temperature change. Upon ultraviolet (UV) light irradiation, a crystal in the β-phase converts to the γ-phase due to the photo-triggered phase transition. The γ-phase achieved by the photo-triggered phase transition forms a unique molecular conformation that cannot be reached via a thermal phase transition. The manifestation mechanism of the photo-triggered phase transition is considered to originate from strain due to the *trans*-keto molecules produced by photoisomerization. The photo-triggered phase transition enables thin enol-(*S*)-**1** crystals to bend stepwise via light irradiation; this phenomenon has the potential to extend the functions of photo-responsive solid materials.

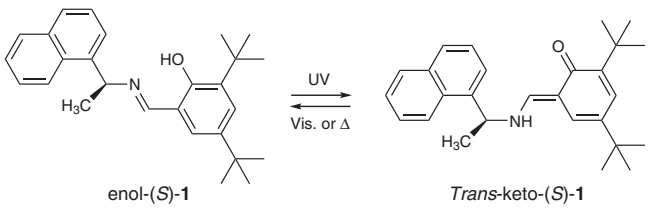

Fig. 1 Enol-keto photoisomerization. Enol form converts into *trans*-keto form by ultraviolet (UV) light irradiation. *Trans*-keto form returns to enol form via thermal back-isomerization or upon visible light irradiation

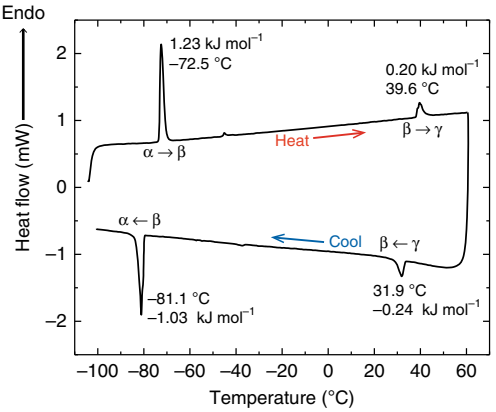

Fig. 2 Differential scanning calorimetry measurement of enol-(*S*)-**1** crystals. DSC curve measured in the temperature range from −100 to 60 °C at a rate of 5 °C min^{-1} on heating and subsequent cooling

Results

Thermal phase transition. Differential scanning calorimetry (DSC) measurement of enol-(*S*)-**1** crystals was performed in the temperature range from −100 to 60 °C at a rate of 5 °C min^{-1} with heating followed by cooling (Fig. 2). On heating, the DSC curve showed two endothermic peaks at −72.5 and 39.6 °C, with enthalpies ΔH of 1.23 and 0.20 kJ mol^{-1}, respectively. On subsequent cooling, the DSC curve showed two exothermic peaks at −81.1 and 31.9 °C, with enthalpies ΔH of −1.03 and −0.24 kJ mol^{-1}, respectively. The thermal hysteresis of each phase transition was 8.6 °C at the low-temperature phase transition α ↔ β, and 7.7 °C at the high-temperature phase transition β ↔ γ. The enthalpy at the phase transition β ↔ γ was approximately one-fifth that of the phase transition α ↔ β, both of which were much smaller than that required for melting at 129.4 °C (Supplementary Fig. 1). These α, β, and γ crystalline phases can be defined as polymorphs of enol-(*S*)-**1** crystal, and the polymorphs appear reversibly due to the low- and high-temperature phase transitions.

X-ray crystallographic analyses of an enol-(*S*)-**1** crystal were performed at various temperatures ranging from −100 to 60 °C, verifying the reversible structural phase transitions among α, β, and γ phases (Fig. 3, Supplementary Tables 1 and 2, and Supplementary Data 1). The crystal structures of α- and β-phases belong to the same space group *P*1. Due to the low-temperature phase transition α → β, the lengths of *a*- and *c*-axes changed by + 1.8 and −1.3% (Fig. 3a, c), respectively, and the *α*, *β*, and *γ* angles decreased by 9°, 5°, and 2.5°, respectively (Fig. 3d–f). In contrast to the α- and β-phases, the crystal structure of the γ-phase belongs to the space group $P2_1$. Although the lengths of the *a*-, *b*-, and *c*-axes changed slightly, by + 0.5, −0.05, and + 0.2%, respectively (Fig. 3a–c), the lattice angles showed a more significant change; *α* and *γ* angles converted to 90° due to a change in the crystal system from triclinic to monoclinic, and *β* increased by + 10° during the high-temperature phase transition β → γ (Fig. 3d–f).

To compare the molecular conformation among α-, β-, and γ-phases, we examined the independent molecules in a unit cell of each phase, as shown in Fig. 4a–f. Two independent molecules, drawn in green and yellow, exist in the lattice in the α-phase (Fig. 4a, d); here, these molecules are referred to as molecule 1 (green) and molecule 2 (yellow). Molecules 1 and 2 form slightly different dihedral angles in salicyl and naphthyl planes, of 54.54° and 52.71° at −90 °C, respectively (Fig. 4g). *Tert*-butyl substituent groups of molecules 1 and 2 in the α-phase are not disordered, forming conformation A (drawn in magenta in Fig. 4a, d, and h).

Molecules 1 and 2 in the β-phase converted to a different conformation from those in the α-phase due to the phase

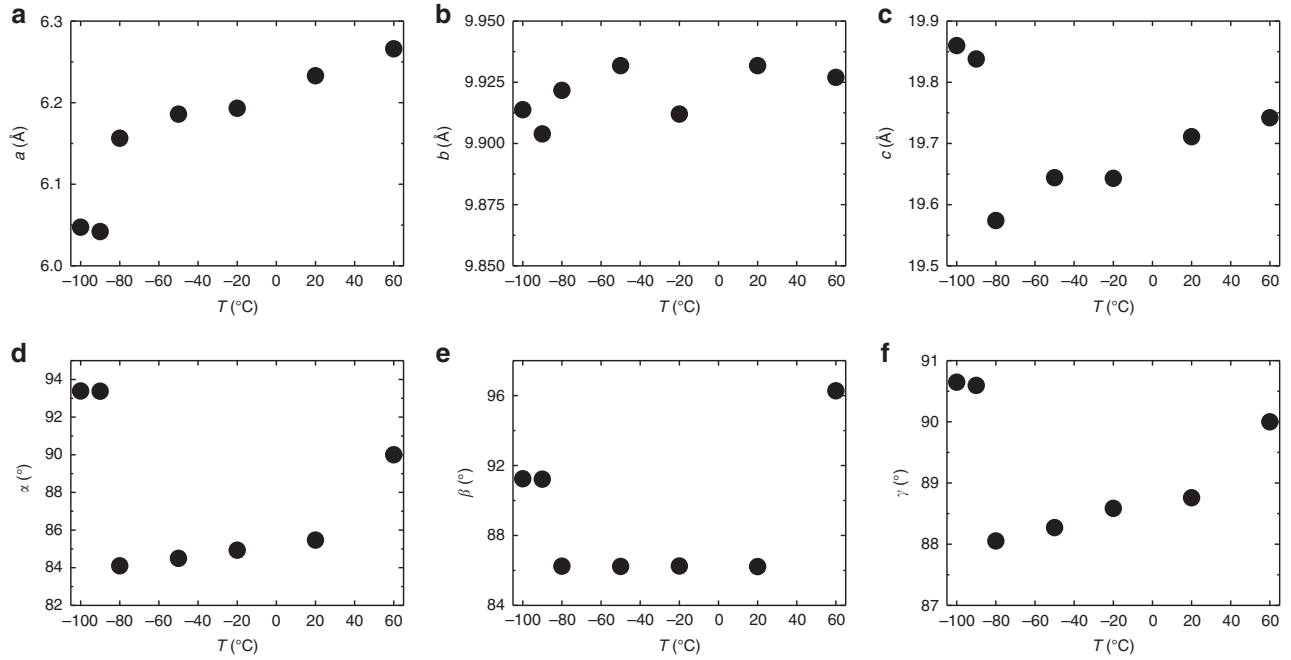

Fig. 3 Crystal structures of the enol-(*S*)-**1** crystal at various temperatures. **a–f** Unit cell parameters of **a** *a*, **b** *b*, and **c** *c*-axes; and **d** *α*, **e** *β*, and **f** *γ* angles

transition α → β (Fig. 4b, e). At −80 °C, the dihedral angles of molecules 1 and 2 were 47.78° and 48.26°, respectively (Fig. 4g), and decreased to 46.40° and 47.58°, respectively, as the temperature increased to 20 °C (Fig. 4g). Another difference from the α-phase is that *tert*-butyl substituent groups of molecules 1 and 2 in the β-phase become disordered, with two conformations, A (magenta) and B (blue) (Fig. 4b). Conformation B is a rotation of nearly 60° from conformation A. The different orientations of *tert*-butyl substituent groups in molecules 1 and 2 are clearly visible in the view parallel to the salicyl plane (Fig. 4e). As to the occupancy of the disordered *tert*-butyl group, conformation A is the main conformation for molecule 1; by contrast, conformation B is the major conformation for molecule 2 in the β-phase (Fig. 4e). The occupancy of conformation A continuously decreases for molecule 1, and increases for molecule 2 with a temperature rise in the β-phase (Fig. 4h).

In the γ-phase, one independent molecule exists in the lattice (Fig. 4c, f). The independent molecule forms a dihedral angle of 46.49° and has conformation A as its major occupancy configuration for the disordered *tert*-butyl group (Fig. 4g, h). This molecular conformation in the γ-phase is relatively similar to molecule 1 in the β-phase, suggesting that the conformation of molecule 2 in the β-phase changed to the same conformation with molecule 1 by changing the dihedral angle and rotating the *tert*-butyl group.

Although molecular conformations are clearly different among α,- β-, and γ-phases, the associated molecular arrangements are similar (Fig. 4i and Supplementary Fig. 2). Molecular packings of the (100) face in the α-, β-, and γ-phases show that the phase transitions α ↔ β and β ↔ γ progress with a slight displacement of each molecule along the *b* axis, inducing changes in the *α*-angle (Fig. 4i). The molecular packings of the (010) and (001) faces are also similar among the three phases (Supplementary Fig. 2). The similarities in the molecular arrangements among α-, β-, and γ-phases can afford structural phase transitions of α ↔ β and β ↔ γ with small transition enthalpies. Due to the structural phase transitions, a plate-like crystal viewed from the (010) face deforms reversibly without any disintegration upon heating and cooling (Supplementary Fig. 3 and Supplementary Movie 1).

Photoisomerization. Ultraviolet-visible (UV–Vis) absorption spectra were measured with a transmittance method to reveal the photochromic nature of the enol-(*S*)-**1** crystal (thickness: 20 μm) in the β- and γ-phases. Without UV light irradiation at 20 °C, the spectrum of the crystal in the β-phase showed a large peak at 300 nm, and almost no absorption above 400 nm (Fig. 5a). Upon weak UV light irradiation (365 nm, 5 mW cm^{-2}), a new peak appeared at 450 nm due to photoisomerization from the enol to *trans*-keto form, with an accompanying crystal color change from yellow to orange (Fig. 5a). The difference spectrum, which was obtained by subtracting the spectrum before UV irradiation from that under UV irradiation, clarified that the absorption increased in the range of 375–550 nm, with a peak at 450 nm (Fig. 5c). The half-life of the thermal back-isomerization from *trans*-keto to enol form was calculated to be 86.2 s, based on the decay curve of the peak intensity at 450 nm after stopping UV irradiation (Fig. 5d). The back-photoisomerization half-life from the *trans*-keto to enol form by visible light (488 nm, 1.4 mW cm^{-2}) was calculated to be 9.9 s using a diffuse reflectance spectrometer (Supplementary Fig. 4). The spectral behavior indicates that back-photoisomerization proceeds much faster than that of thermal back-isomerization.

At 50 °C, the spectrum of the crystal in the γ-phase under UV irradiation did not change significantly from that before UV irradiation (Fig. 5b). Although the difference spectrum failed to provide any discernible new peak in the range of 375–550 nm, the time dependence at 450 nm indicated that the absorption intensity upon UV irradiation increased slightly from that before UV irradiation, suggesting photoisomerization with considerably lower conversion in the γ-phase than that in the β-phase (Fig. 5c, d).

Photo-triggered phase transition. Surprisingly, when the unit cell parameters of an enol-(*S*)-**1** crystal (0.4 × 0.4 × 0.08 mm^3) were measured during UV irradiation (365 nm, 60 mW cm^{-2}), the unit cell of the β-phase converted to that of the γ-phase (Fig. 6). Here, the change in the *α*-angle is an indicator of the photo-triggered phase transition, because the *α*-angle changes the most during the α → β transition, reaching 90° with the β → γ

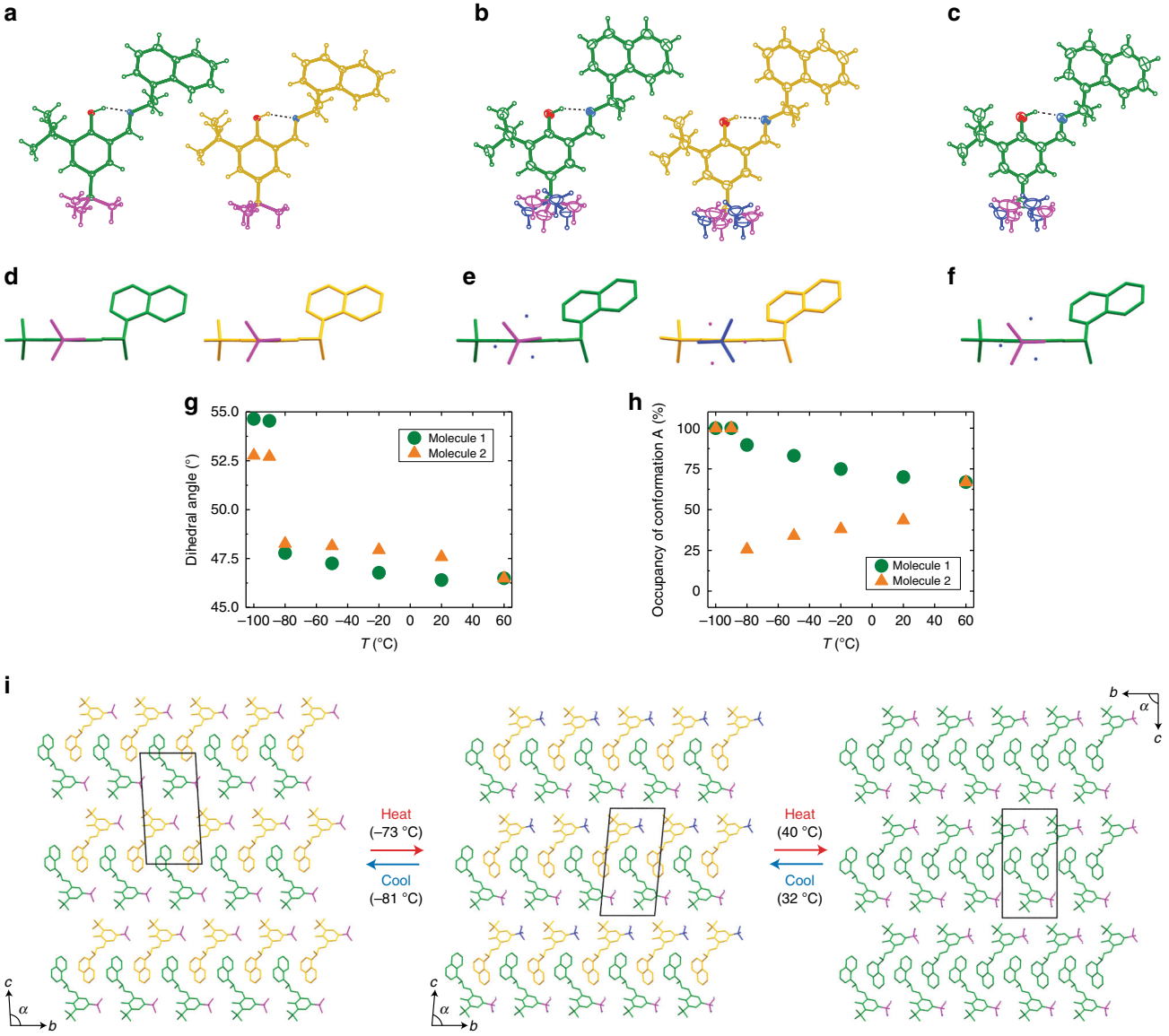

Fig. 4 Crystal structures of the enol-(*S*)-**1** crystal in the three phases. **a–f** Molecular conformations of independent molecules at **a**, **d** α-, **b**, **e** β-, and **c**, **f** γ-phases. **a–c** ORTEP figures are drawn by thermal ellipsoids with 25% probability. Two independent molecules in α- and β-phases are shown in green (molecule 1) and yellow (molecule 2), and an independent molecule in the γ-phase is drawn in green due to its similarity to molecule 1. The conformations of disordered *tert*-butyl substituents are shown in magenta (conformation A) and blue (conformation B). **d–f** Molecular conformations viewed parallel to the salicyl plane. Hydrogen atoms and *tert*-butyl bonds with minor occupancy are omitted for clarity. **g** Dihedral angle between salicyl and naphthyl planes. **h** Occupancy of conformation A of disordered *tert*-butyl substituents. **i** Molecular packings on the (100) face at α-, β-, and γ-phases

transition. The α-angle in the β-phase changed to 90° under UV irradiation at various temperatures of −50, −20, 0, and 20 °C (Fig. 6a). In contrast to the change that occurred in the β-phase, the α-angle measured at −120 °C (α-phase) and 60 °C (γ-phase) did not change under UV irradiation (Fig. 6a). The directions of the phase transitions are schematically summarized (Fig. 6b). The β- and γ-angles also coincided with those corresponding to the γ-phase, accompanied by a slight length change in the *a*-, *b*-, and *c*-axes (Fig. 6c). These results suggest that UV light irradiation triggers the β → γ transition, but not the α → β phase transition.

Interestingly, when a thick enol-(*S*)-**1** crystal ($2010 \times 1235 \times 737\ \mu m^3$) was irradiated by UV light (365 nm, 80 mW cm^{-2}) at room temperature (β-phase), we could clearly see the phase transition β ↔ γ under a microscope, as follows. The crystal started to transform from the irradiated (001) surface upon UV irradiation, and then the phase boundary propagated in the opposite direction (Fig. 7a and Supplementary Movie 2). The angle between the (001) and (012) faces at the upper right edge changed from 47° to 45° (Fig. 7a, c). The transformation continued to propagate to a lower direction within 1 s, and the angle between $(0\bar{1}\bar{1})$ and $(00\bar{1})$ at the lower left edge changed from 67° to 63° (Fig. 7a, c). The deformed shape after UV irradiation corresponded to the crystal shape of the γ-phase (Fig. 7c). The propagation speed of the phase boundary was calculated as 920 μm s^{-1} at 80 mW cm^{-2} UV light intensity. The propagation speed slowed with a reduction in the light intensity, and the deformation was incomplete for the weaker light intensity of 20 mW cm^{-2} (Supplementary Fig. 5). These results indicate that there is a threshold UV light intensity to realize the photo-triggered phase transition.

After stopping UV irradiation, the crystal maintained its deformed shape for 50 s. Then, the phase boundary appeared,

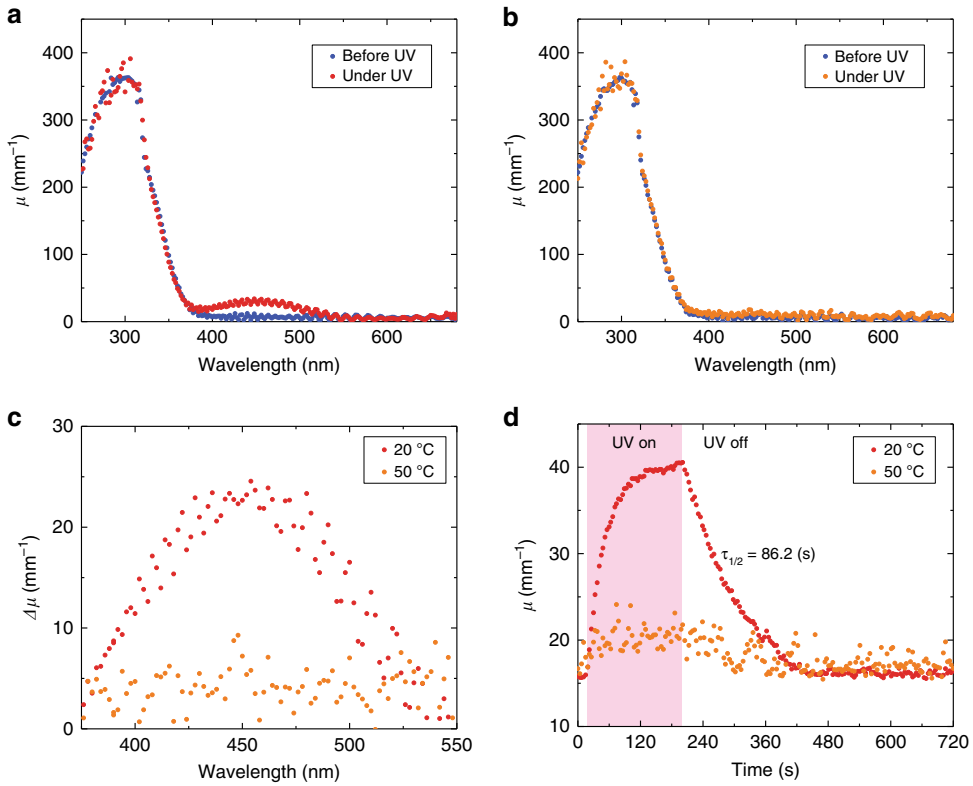

Fig. 5 Ultraviolet (UV)–visible (Vis) absorption spectra of the enol-(*S*)-**1** crystal. **a**, **b** UV–Vis absorption spectra of an enol-(*S*)-**1** crystal (thickness: 20 μm) on the (001) top face before and under UV light irradiation (365 nm, 5 mW cm^{-2}) at **a** 20 and **b** 50 °C. **c** Difference spectra at 20 and 50 °C obtained by subtracting the spectrum before UV light irradiation from that under UV light irradiation. **d** Time dependence of the absorption at 450 nm under on–off UV light irradiation at 20 and 50 °C. In each panel, the absorption was expressed in terms of the absorption coefficient for normalization

with the return of the angle at the lower left edge from 63° to 67° (50 s, Fig. 7b). The phase boundary gradually progressed to the upper direction (70 s, Fig. 7b), and then the entire crystal returned to its initial shape in the β-phase (110 s, Fig. 7b) The propagation speed of the reverse deformation is roughly consistent with the speed of thermal back-isomerization from the *trans*-keto to enol form (Fig. 5d).

To clarify the photothermal effect by UV light, the surface temperature of an enol-(*S*)-**1** crystal was monitored with an infrared (IR) thermography camera (Fig. 7d, e). When the crystal was irradiated with UV light (365 nm, 80 mW cm^{-2}), the irradiated surface temperature rose from 22.6 to 26.8 °C in 0.2 s, at which the photo-triggered transformation already started (Fig. 7a, e). Then, the surface temperature continued to increase to 37.5 °C in 1 s, at which the transformation completed (Fig. 7a, d, e). Thus, this temperature measurement revealed that the photo-triggered transformation progressed before reaching the thermal phase transition temperature.

After stopping the UV irradiation, the surface temperature decreased to the initial temperature in 5 s (Fig. 7e). The time scale of the temperature decrease was much faster than the crystal shape recovery (Fig. 7b). These results suggest that the photo-triggered phase transition β → γ is triggered by enol–keto photoisomerization, and the reverse transition γ → β occurs due to back-isomerization.

When the photoirradiation continued for 20 s, the surface temperature increased by nearly 30 °C in 5 s, and then kept a steady state during 5–20 s (Supplementary Fig. 6). This result indicates that a crystal temperature will not increase above the phase transition temperature during low-temperature X-ray measurements.

Crystal structure change upon UV irradiation. To elucidate the structural difference of γ-phase formed by the photo-triggered phase transition and the thermal phase transition, the crystal structures were determined using the same sample shown in Supplementary Fig. 7 before and under UV irradiation at −50 and 50 °C (Fig. 8, Supplementary Tables 3 and 4, and Supplementary Data 2). The crystal structures of the β- and γ-phases without UV irradiation are described in detail in a previous section. Under UV light irradiation at −50 °C, the crystal structure of the β-phase changed to that of the γ-phase; the *trans*-keto molecule was not found, likely due to insufficient quantities for structural determination. However, the enol-(*S*)-**1** molecule in the γ-phase achieved by a photo-triggered phase transition has a slightly different conformation from that of the γ-phase achieved by simple heating. The molecule under UV irradiation at −50 °C forms a dihedral angle of 47.4°, and the occupancy of the disordered *tert*-butyl group is A:B = 90:10 (Fig. 8b). By contrast, the molecule without UV light at 50 °C forms a dihedral angle of 46.6°, and the occupancy of the disordered *tert*-butyl group is A:B = 71:29 (Fig. 8c). The conformational difference reflects on the temperature difference, as the dihedral angle decreases to 46.6° and the occupancy of the disorder approaches A:B = 71:29, depending on the temperature rise (Fig. 4g, h). The molecular conformation under UV light at 50 °C did not change from that before UV irradiation (Fig. 8c, d). Thus, the γ-phase achieved by the photo-triggered phase transition is a unique state with respect to molecular conformation, which cannot be achieved by thermal phase transition. To our knowledge, this is the first evidence of this kind of photo-triggered phase transition.

Subsequently, the time dependence of unit cell changes after stopping the UV light irradiation was measured at −50 °C

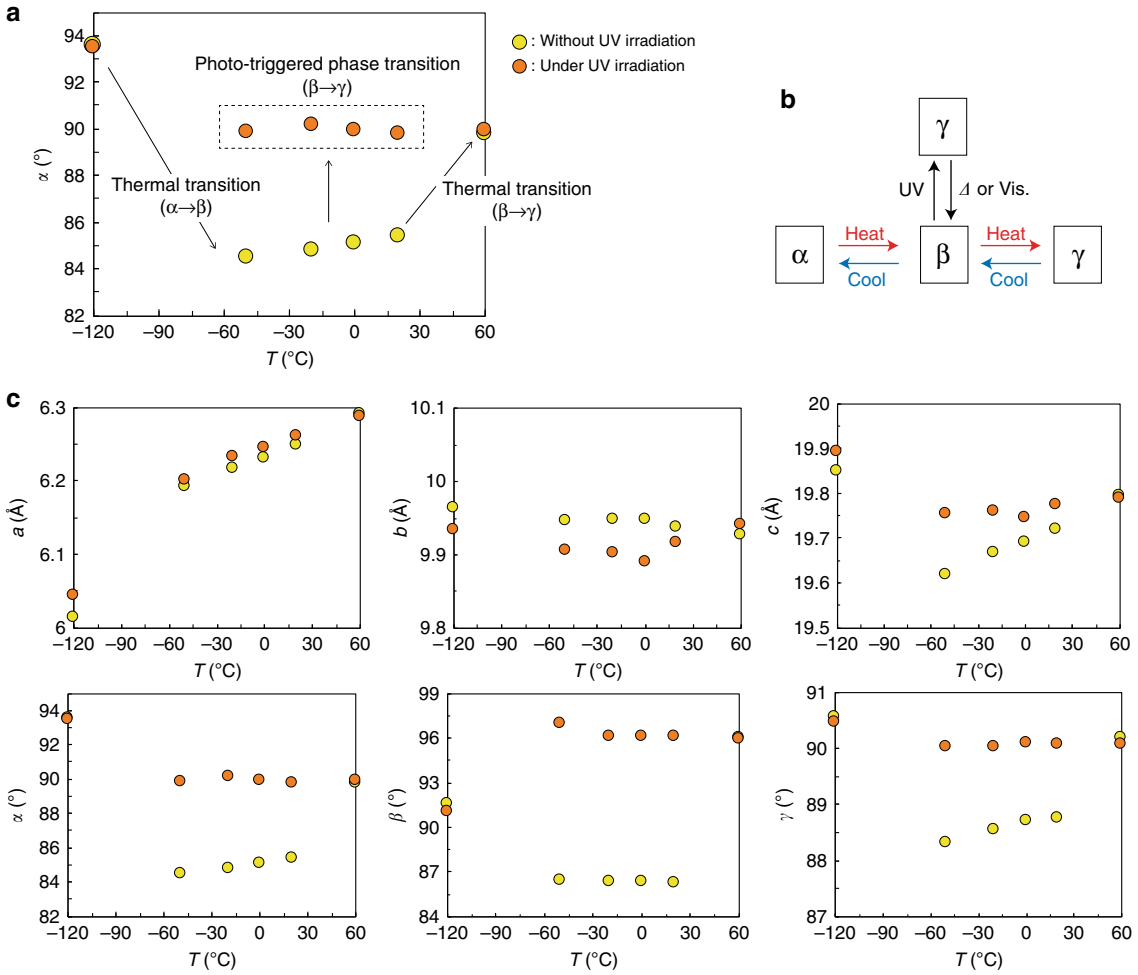

Fig. 6 Lattice change upon ultraviolet (UV) light irradiation at various temperatures. **a** Photo-triggered phase transition based on the α-angle change. **b** Diagram of the phase change due to temperature change and photoirradiation. **c** Unit cell parameters of *a*-, *b*-, *c*-axes; and α-, β-, and γ-angles. The yellow and orange circles indicate the results without and under UV irradiation, respectively

(Supplementary Figs. 8 and 9). For instance, the α-angle, which becomes 90° due to the photo-triggered phase transition β → γ, maintained 90° at least 80 min after stopping the irradiation (Supplementary Fig. 8). By contrast, when the crystal was irradiated by visible light (488 nm, 10 mW cm^{-2}) just after stopping the UV light irradiation, the α-angle returned to 85° in the β-phase within 20 min (Supplementary Fig. 9). Faster return of the unit cell under visible light corresponds to back-photoisomerization, which is much faster than thermal back-isomerization (Supplementary Fig. 4). These lattice change behaviors, with and without visible light, verify that the phase transition γ → β is triggered by back-isomerization from the *trans*-keto to enol form.

Stepwise bending. From the perspective of actuation behavior, the photo-triggered phase transition should lead to stepwise bending (Fig. 9 and Supplementary Movie 3). When the (001) face of a thin plate-like enol-(*S*)-**1** crystal (4072 × 940 × 36 μm^3) in the β-phase was irradiated from the left with UV light (365 nm, 60 mW cm^{-2}) at room temperature, the crystal bent towards the light source with a twisting motion in 0.2 s, accompanied by a color change from yellow to orange (Fig. 9a, b). In the next moment, the bent crystal suddenly released its twisting motion (Fig. 9c). Then, the crystal continued to bend towards the light source without twisting under prolonged UV irradiation (Fig. 9d). After stopping light irradiation, the bending gradually returned without twist in 45 s (Fig. 9e). The bent crystal started to twist slowly, and then exhibited its most twisted shape at 70 s (Fig. 9f). The bending with a twist gradually relaxed, and then the crystal returned to its initial straight shape and its color returned to yellow (Fig. 9g).

The bending behavior during the process described above can be divided into three steps: (1) bending with twisting due to enol–keto photoisomerization at the β-phase, (2) the disappearance of the twist due to the photo-triggered phase transition β → γ, and (3) bending without twisting due to enol–keto photoisomerization in the γ-phase. The motion of each step was confirmed by applying weak UV light and IR light heating separately (Supplementary Fig. 10). Thermal relaxation of the bending behavior can be explained by the reverse process. Bending relaxation without twist occurs due to thermal back-isomerization in the γ-phase. Then, twisting motion gradually appears due to the progression of the phase transition γ → β triggered by thermal back-isomerization. The bending with a twist returns to the initial unbent shape due to thermal back-isomerization in the β-phase.

The stepwise bending was repeatable at least 40 cycles without disintegration, but in some cases, crystals cracked along the width direction of *a* axis (Supplementary Fig. 11). The crack should be generated by the strain of surface contraction along the length direction of *b* axis, which is consistent to the bending towards the light source.

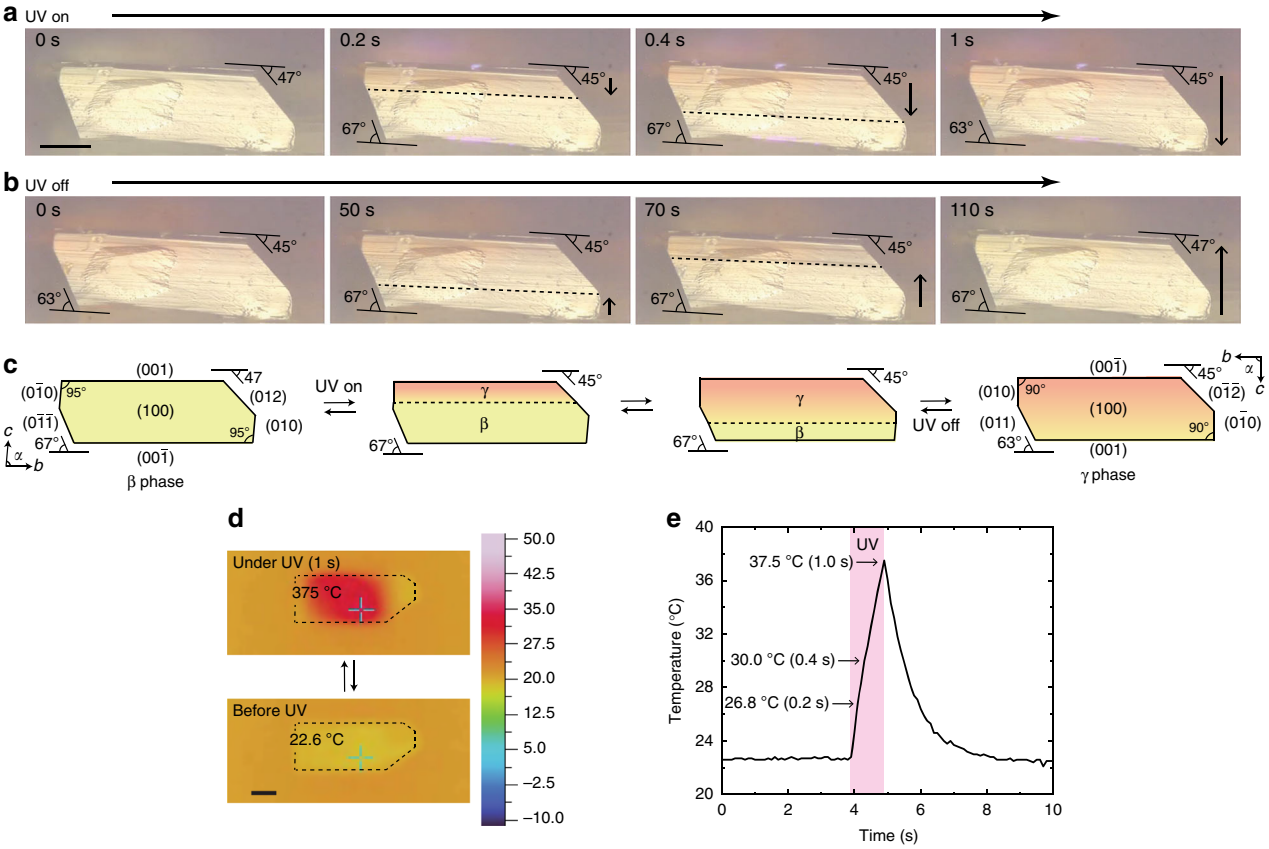

Fig. 7 Photo-triggered transformation and surface temperature measurement. **a**, **b** Photo-triggered transformation of a thick plate-like crystal of enol-(*S*)-**1** **a** upon ultraviolet (UV) light irradiation and **b** after stopping the irradiation (Supplementary Movie 2). Dotted lines indicate the propagation of the phase boundary. The scale bar is 0.5 mm. **c** Schematic illustration of the photo-triggered transformation. **d** Crystal surface temperature change upon UV light irradiation for 1 s monitored by an infrared (IR) thermography camera. The scale bar is 1 mm. **e** Time dependence of the surface temperature change at the cross point shown in **d**

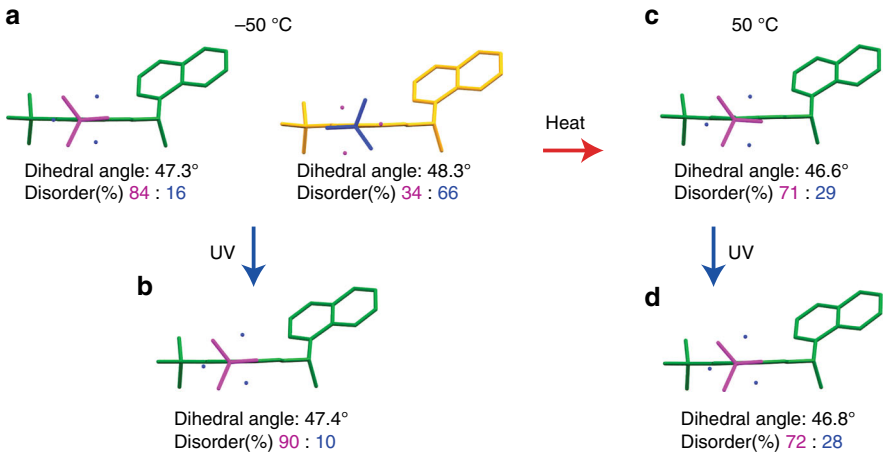

Fig. 8 Crystal structure change due to the photo-triggered phase transition. **a–d** Molecular conformation **a** without and **b** under ultraviolet (UV) light at −50 °C, and **c** without and **d** under UV light at 50 °C. Two independent molecules in the β-phase are shown in green (molecule 1) and yellow (molecule 2); an independent molecule in the γ-phase is drawn in green due to the similarity to molecule 1 of the β-phase. *Tert*-butyl substituent is disordered between two conformations drawn in magenta and blue. Dots represent the minor orientation of the disordered *tert*-butyl substituent. Hydrogen atoms are omitted for clarity. Crystallographic data are summarized in Supplementary Table 3

Discussion

To consider the structural changes due to photoisomerization, the structures of enol, *trans*-keto, and *cis*-keto forms were optimized by density functional theory calculations at the theory level of B3LYP/6-31G (Fig. 10a)[31]. The optimized structure of enol-(*S*)-**1** with a dihedral angle of 56° was consistent with X-ray crystallographic results for the enol-(*S*)-**1** crystal; *cis*-keto-(*S*)-**1** was similar to enol-(*S*)-**1**. By contrast, the structure of *trans*-keto-(*S*)-**1** differed significantly from enol-(*S*)-**1**, forming a dihedral angle of 85°. This structural difference between enol and *trans*-keto

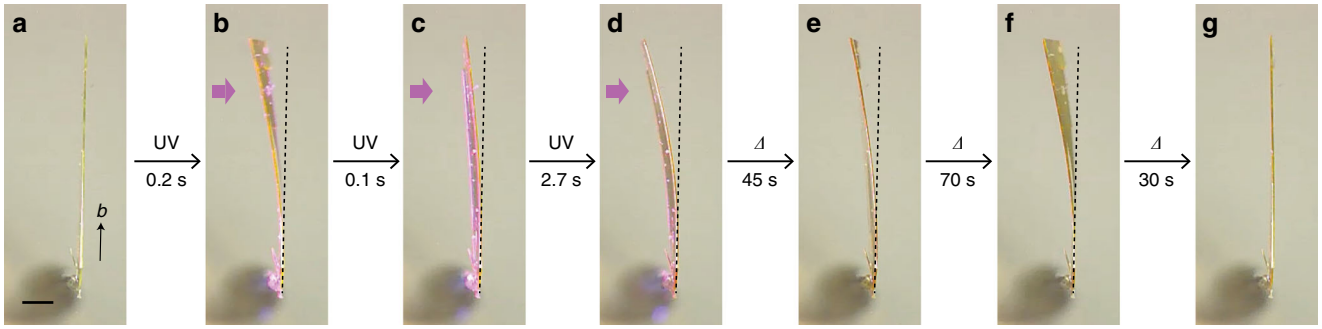

Fig. 9 Stepwise bending of a thin plate-like crystal of enol-(*S*)-**1** upon photoirradiation. **a**–**g** Snapshots of the stepwise bending from the side view of the plate-like crystal (Supplementary Movie 3). **a**, **b** Fast bending with twisting of the β-phase upon ultraviolet (UV) light irradiation. **c** Sudden disappearance of the twist due to the photo-triggered phase transition β → γ. **d** Bending without twist of the γ-phase under UV light irradiation. **e** Thermal relaxation of the bending without twist in the γ-phase. **f** Gradual appearance of twist due to the reverse phase transition γ → β. **g** Returning to the initial shape at the β-phase. The scale bar is 0.5 mm

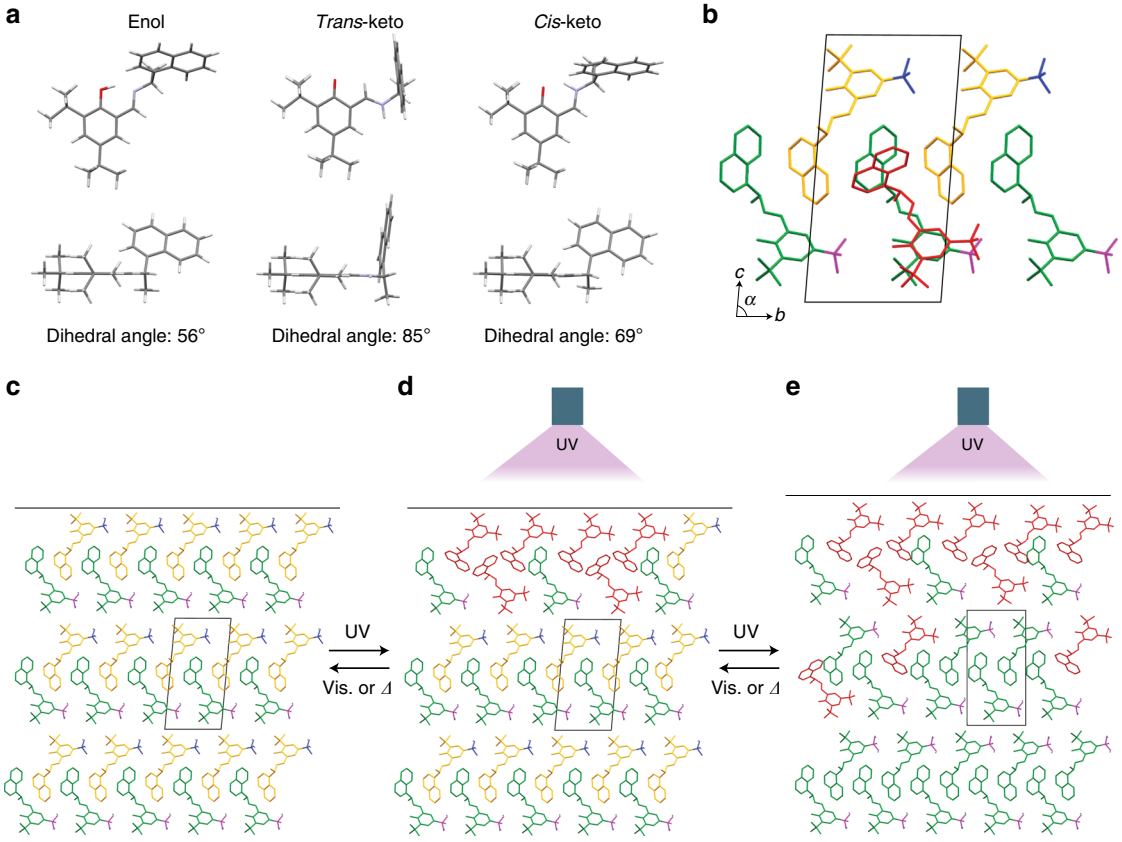

Fig. 10 Possible mechanism of photo-triggered phase transition. **a** Molecular structure of enol, *trans*-keto, and *cis*-keto molecules viewed perpendicular and parallel to the salicyl plane obtained by density functional theory calculations. **b** Overlay of a *trans*-keto molecule on the (001) face of the enol-(*S*)-**1** crystal in the β-phase. Two independent molecules in the β-phase drawn in yellow and green; the *trans*-keto molecule is drawn in red. **c** (001) Plane view of the β-phase before UV irradiation. **d** Photoisomerization of the crystal in the β-phase. **e** Photo-triggered phase transition β → γ due to the strain of *trans*-keto molecules

forms suggests that photoisomerization from the enol to *trans*-keto form undergoes by pedal motion in a limited space[32] and generates strain in the crystal (Fig. 10b).

Photoisomerization should lead to a photo-triggered phase transition (Fig. 10c–e). The enol-(*S*)-**1** crystal before photo-irradiation is in the β-phase (Fig. 10c). Upon UV irradiation, *trans*-keto molecules are produced due to photoisomerization at the irradiated surface, generating strain in the crystal (Fig. 10d). The strain due to *trans*-keto molecules induces conformational change of the surrounding molecules. The conformational change further influences the adjacent surrounding molecules, similar to a domino effect, triggering crystal structure change from the β- to γ-phase (Fig. 10e). When *trans*-keto molecules are produced at a certain low ratio, the whole crystal completes the phase transition into the γ-phase. When the light irradiation stops, thermal back-isomerization from the *trans*-keto to the enol form occurs in the crystal, triggering the reverse phase transition γ → β (Fig. 10d).

This transition mechanism indicates that the γ-phase reached by the photo-triggered phase transition requires *trans*-keto molecules to maintain the crystal phase. In fact, the phase

transition γ → β under visible light irradiation proceeds faster than that without visible light, due to the half-life of back-photoisomerization from the *trans*-keto to the enol form, which is much shorter than that of thermal back-isomerization.

As such, *trans*-keto molecules are the source of strain in a crystal and the conversion ratio is crucial to analyze quantitatively the photo-triggered phase transition. However, it is impossible to obtain the conversion ratio in this case, because the pure *trans*-keto molecule cannot be isolated due to spontaneous thermal back-isomerization. As an estimation, the conversion ratio might be at most 5% or so, based on the insufficient amount for X-ray structure determination. In addition, the generated strain from *trans*-keto molecules is difficult to calculate due to bending with a twist. As our future work, experimental measurement of strain–stress relationship produced by *trans*-keto molecules is required for quantitative analysis of the photo-triggered phase transition.

The manifestation of the photo-triggered phase transition should also be correlated with enthalpy, which is the energy barrier required for the phase transition. The enthalpy at the phase transition β → γ (0.2 kJ mol^{-1}) is one-fifth smaller than that at the phase transition α → β (1 kJ mol^{-1}). The difference in these transition enthalpies supports that enol–keto photo-isomerization triggers the phase transition β → γ, but does not trigger the phase transition α → β due to a larger enthalpy. The enthalpy at the phase transition β → γ is also smaller than other structural phase transitions of molecular crystals[18,21,24,30,33–35].

Additionally, enthalpy at the transition β → γ is 10–200 times larger than the energy densities of superelastic and ferroelastic molecular crystals, which can deform with the creation of a new crystalline phase or twin domains by manually applying shear stress[36–39]. This suggests that it will be difficult to create the γ-phase by shear stress in the enol-(*S*)-**1** crystal at the β-phase. In fact, we did not see any deformation of the enol-(*S*)-**1** crystal when manually applying stress under a microscope.

Finally, we would like to discuss the difference between the photo-triggered phase transition described in this paper and the photo-induced phase transition that appears in the literatures[7–10]. The crystal phase due to the photo-induced phase transition appears only by light irradiation, which changes the electric and/or magnetic properties of the crystals within femto- or picoseconds. Regarding the photo-triggered phase transition, the crystal phase triggered by light is identical to that via a thermal phase transition, induced by heating, but unique with respect to its molecular conformation. Thus, the photo-triggered phase transition may lead to a new strategy to broaden the applicability of photo-responsive solids.

Methods

Material preparation. An enol-(*S*)-**1** compound was synthesized using microwaves (Monowave 300, Anton Paar, Graz, Austria), according to the literature[40]. Plate-like single crystals of enol-(*S*)-**1** were obtained by evaporation of 2-propanol or acetonitrile solution at ambient temperature.

Thermal analysis. DSC measurements were conducted with a differential scanning calorimeter (Thermo plus EVO2 DSCvesta, Rigaku) at a speed of 5 °C min^{-1} in the temperature range from −100 to 60 °C. Another calorimeter (DSC 8500, Perkin Elmer, Waltham, MA, USA) was also employed for measurements in the range of 30–160 °C. The molar transition enthalpy Δ*H* was calculated based on the peak area under the DSC curve from the baseline.

UV–Vis absorption measurement. Absorption spectra of an enol-(*S*)-**1** crystal were measured using a transmittance method[41]. A thin plate-like crystal prepared by solvent evaporation was fixed on a Cu plate with a pinhole of diameter of ~0.5 mm. Transmitted light intensity through the sample was measured over the range of 250–680 nm at 2-nm resolution. Transmitted light intensity through the Cu plate without a sample was also measured in the same wavelength range for blanks. UV–Vis absorption spectra were calculated according to the Beer–Lambert–Bouguer law, and then divided by the crystal thickness to obtain the absorption coefficient for standardization. Sample temperature was regulated by a Peltier thermostat. A diffuse reflectance spectrometer (Lambda 650, Perkin Elmer) was also employed to measure the spectral behavior upon visible light irradiation ($\lambda = 488$ nm, FOLS-2, Sawaki Kobo).

X-ray crystallographic analysis. Single-crystal X-ray diffraction data of enol-(*S*)-**1** without UV light at various temperatures were collected using a R-AXIS RAPID diffractometer (Rigaku) equipped with monochromatic Mo-Kα radiation ($\lambda =$ 0.71075 Å) at 50 kV and 40 mA. The temperature of the sample was regulated using a N_2 gas flow cryostat and calibrated with a thermocouple. Unit cell parameters before, under, and after UV light irradiation were also measured with this diffractometer. The light irradiation was performed with a UV-LED lamp ($\lambda = 365$ nm, UV-400, Keyence, Osaka, Japan) and LD light source ($\lambda = 488$ nm, FOLS-2, Craft Center SAWAKI Inc.). Crystal structures before and under UV light irradiation at −50 and 50 °C were determined using an XtaLAB Synergy diffractometer (Rigaku) equipped with monochromatic Cu-Kα radiation ($\lambda = 1.54187$ Å). The crystal structures were solved using a direct method with SHELXS2013[42] or SHELXD2013[42], and then refined on F^2 using the full-matrix least-squares method of SHELXL[42]. Calculations were performed using the Rigaku crystal structure software package[43] and a graphical interface, ShelXle[44].

Observation of mechanical behavior of crystals. Shape change upon heating and cooling was observed using a temperature control stage (Japan High Tech) and a digital high-speed microscope (VHX-500, Keyence). Shape change and bending behavior of enol-(*S*)-**1** crystals upon UV light irradiation ($\lambda = 365$ nm, UV-400, Keyence) were observed at room temperature using the digital high-speed microscope. Surface temperature change upon UV light irradiation was measured with an IR thermography camera (FSV-2000, Apiste) in a super dry room. The substrate temperature of the glass plate was regulated with a Peltier thermo-controller (VPE-35, VICS).

Data availability

The crystallographic data have been deposited at the Cambridge Crystallographic Data Center (CCDC) as CCDC 1879558–1879568 and can be obtained free of charge from the CCDC via www.ccdc.cam.ac.uk/getstructures. All other data are available from the corresponding author upon reasonable request.

Received: 27 November 2018 Accepted: 28 January 2019
Published online: 20 February 2019

References

1. Cohen, R. E. Origin of ferroelectricity in perovskite oxides. *Nature* **358**, 136–138 (1992).
2. Smith, M. B. et al. Crystal structure and the paraelectric-to-ferroelectric phase transition of nanoscale $BaTiO_3$. *J. Am. Chem. Soc.* **130**, 6955–6963 (2008).
3. Wu, Z. & Cohen, R. E. Pressure-induced anomalous phase transitions and colossal enhancement of piezoelectricity in $PbTiO_3$. *Phys. Rev. Lett.* **95**, 037601 (2005).
4. Maat, S., Thiele, J. U. & Fullerton, E. E. Temperature and field hysteresis of the antiferromagnetic-to-ferromagnetic phase transition in epitaxial FeRh films. *Phys. Rev. B* **72**, 214432 (2005).
5. Pons, J., Chernenko, V. A., Santamarta, R. & Cesari, E. Crystal structure of martensitic phases in Ni–Mn–Ga shape memory alloys. *Acta Mater.* **48**, 3027–3038 (2000).
6. Otsuka, K. & Ren, X. Physical metallurgy of Ti–Ni-based shape memory alloys. *Prog. Mater. Sci.* **50**, 511–678 (2005).
7. Koshihara, S., Tokura, Y., Takeda, K. & Koda, T. Reversible photoinduced phase transitions in single crystals of polydiacetylenes. *Phys. Rev. Lett.* **68**, 1148–1151 (1992).
8. Fukazawa, N. et al. Charge and structural dynamics in photoinduced phase transition of $(EDO\text{-}TTF)_2PF_6$ examined by picosecond time-resolved vibrational spectroscopy. *J. Phys. Chem. C.* **116**, 5892–5899 (2012).
9. Gao, M. et al. Mapping molecular motions leading to charge delocalization with ultrabright electrons. *Nature* **496**, 343–346 (2013).
10. Morrison, V. R. et al. A photoinduced metal-like phase of monoclinic VO_2 revealed by ultrafast electron diffraction. *Science* **346**, 445–448 (2014).
11. Kuwahara, H., Tomioka, Y., Asamitsu, A., Moritomo, Y. & Tokura, Y. A first-order phase transition induced by a magnetic field. *Science* **270**, 961–963 (1995).
12. Jeong, J. et al. Suppression of metal-insulator transition in VO_2 by electric field–induced oxygen vacancy formation. *Science* **339**, 1402–1405 (2013).

13. Maji, T. K., Mostafa, G., Matsuda, R. & Kitagawa, S. Guest-induced asymmetry in a metal-organic porous solid with reversible single-crystal-to-single-crystal structural transformation. *J. Am. Chem. Soc.* **127**, 17152–17153 (2005).
14. Scott, J. F. Applications of modern ferroelectrics. *Science* **315**, 954–959 (2007).
15. Song, G., Ma, N. & Li, H. N. Applications of shape memory alloys in civil structures. *Eng. Struct.* **28**, 1266–1274 (2006).
16. Irie, M., Fukaminato, T., Matsuda, K. & Kobatake, S. Photochromism of diarylethene molecules and crystals: memories, switches, and actuators. *Chem. Rev.* **114**, 12174–12277 (2014).
17. Naumov, P., Chizhik, S., Panda, M. K., Nath, N. K. & Boldyreva, E. Mechanically responsive molecular crystals. *Chem. Rev.* **115**, 12440–12490 (2015).
18. Yao, Z. S. et al. Molecular motor-driven abrupt anisotropic shape change in a single crystal of a Ni complex. *Nat. Chem.* **6**, 1079–1083 (2014).
19. Liu, G., Liu, J., Liu, Y. & Tao, X. Oriented single-crystal-to-single-crystal phase transition with dramatic changes in the dimensions of crystals. *J. Am. Chem. Soc.* **136**, 590–593 (2013).
20. Minami, T., Sato, H. & Matsumoto, S. Macroscopic crystalline deformation in an organic dye during reversible phase transition caused by alkyl disorder. *CrystEngComm* **20**, 2644–2647 (2018).
21. Shima, T. et al. Thermally driven polymorphic transition prompting a naked-eye-detectable bending and straightening motion of single crystals. *Angew. Chem. Int. Ed.* **53**, 7173–7178 (2014).
22. Sahoo, S. C., Panda, M. K., Nath, N. K. & Naumov, P. Biomimetic crystalline actuators: structure–kinematic aspects of the self-actuation and motility of thermosalient crystals. *J. Am. Chem. Soc.* **135**, 12241–12251 (2013).
23. Panda, M. K. et al. Colossal positive and negative thermal expansion and thermosalient effect in a pentamorphic organometallic martensite. *Nat. Commun.* **5**, 4811 (2014).
24. Taniguchi, T. et al. Walking and rolling of crystals induced thermally by phase transition. *Nat. Commun.* **9**, 538 (2018).
25. Kobatake, S., Takami, S., Muto, H., Ishikawa, T. & Irie, M. Rapid and reversible shape changes of molecular crystals on photoirradiation. *Nature* **446**, 778–781 (2007).
26. Koshima, H., Ojima, N. & Uchimoto, H. Mechanical motion of azobenzene crystals upon photoirradiation. *J. Am. Chem. Soc.* **131**, 6890–6891 (2009).
27. Kim, T., Al-Muhanna, M. K., Al-Suwaidan, S. D., Al-Kaysi, R. O. & Bardeen, C. J. Photoinduced curling of organic molecular crystal nanowires. *Angew. Chem. Int. Ed.* **52**, 6889–6893 (2013).
28. Kitagawa, D., Nishi, H. & Kobatake, S. Photoinduced twisting of a photochromic diarylethene crystal. *Angew. Chem. Int. Ed.* **52**, 9320–9322 (2013).
29. Taniguchi, T., Fujisawa, J., Shiro, M., Koshima, H. & Asahi, T. Mechanical motion of chiral azobenzene crystals with twisting upon photoirradiation. *Chem. Eur. J.* **22**, 7950–7958 (2016).
30. Kitagawa, D., Kawasaki, K., Tanaka, R. & Kobatake, S. Mechanical behavior of molecular crystals induced by combination of photochromic reaction and reversible single-crystal-to-single-crystal phase transition. *Chem. Mater.* **29**, 7524–7532 (2017).
31. Frisch, M. J. et al. *Gaussian 09, Rev. B.01*. (Gaussian, Inc., Wallingford, USA, CT, 2010).
32. Harada, J., Uekusa, H. & Ohashi, Y. X-ray analysis of structural changes in photochromic salicylideneaniline crystals. *Solid-State React. Induc. two-Photon Excit. J. Am. Chem. Soc.* **121**, 5809–5810 (1999).
33. Takanabe, A. et al. Reversible single-crystal-to-single-crystal phase transition of chiral salicylidenephenylethylamine. *Crystals* **7**, 7 (2016).
34. Nath, N. K. et al. Single-crystal-to-single-crystal transition in an enantiopure [7] helquat salt: the first observation of a reversible phase transition in a helicene-like compound. *Chem. Eur. J.* **21**, 13508–13512 (2015).
35. Dharmarwardana, M. et al. Thermo-mechanically responsive crystalline organic cantilever. *Chem. Commun.* **53**, 9890–9893 (2017).
36. Takamizawa, S. & Miyamoto, Y. Superelastic organic crystals. *Angew. Chem. Int. Ed.* **53**, 6970–6973 (2014).
37. Takamizawa, S. & Takasaki, Y. Superelastic shape recovery of mechanically twinned 3,5-difluorobenzoic acid crystals. *Angew. Chem. Int. Ed.* **54**, 4815–4817 (2015).
38. Mir, S. H., Takasaki, Y., Engel, E. R. & Takamizawa, S. Ferroelasticity in an organic crystal: a macroscopic and molecular level study. *Angew. Chem. Int. Ed.* **56**, 15882–15885 (2017).
39. Engel, E. R. & Takamizawa, S. Versatile Ferroelastic deformability in an organic single crystal by twinning about a molecular zone axis. *Angew. Chem. Int. Ed.* **57**, 11888–11892 (2018).
40. Smith, H. E., Cook, S. L. & Warren, M. E. Jr. Optically active amines. II. The optical rotatory dispersion curves of the N-benzylidene and substituted N-benzylidene derivatives of some open-chain primary amines. *J. Org. Chem.* **29**, 2265–2272 (1964).
41. Takanabe, A. et al. Optical activity and optical anisotropy in photomechanical crystals of chiral salicylidenephenylethylamines. *J. Am. Chem. Soc.* **138**, 15066–15077 (2016).
42. Sheldrick, G. M. A short history of SHELX. *Acta Crystallogr. A.* **64**, 112–122 (2008).
43. CrystalStructure v.4. 2. 2. (Rigaku Corporation, Tokyo, Japan, 2016).
44. Hübschle, C. B., Sheldrick, G. M. & Dittrich, B. ShelXle: a Qt graphical user interface for SHELXL. *J. Appl. Cryst.* **44**, 1281–1284 (2011).

Acknowledgements

This study was financially supported by the JSPS Grant-in-Aid for Scientific Research B (17H03107), Challenging Exploratory Research (16K12918), and Research Fellowship for Young Scientists, and WISE project research (Research for Energy-Next) at Waseda University. We would like to thank Japan High Tech Co., Ltd. for the use of a temperature control stage. We also thank Smart Energy System Innovation Center at Waseda University for the use of a super dry room. T.T. and T.A. thanks the Leading Graduate Program in Science and Engineering at Waseda University.

Author contributions

T.T. and H.K. planned the experiments and wrote the paper. H.S. measured crystal structure under light irradiation. Y.H. measured absorption spectral change by visible light. T.T. performed all other experiments and analyses. H.K. and T.A. managed the project.

Additional information

Supplementary information accompanies this paper at https://doi.org/10.1038/s42004-019-0121-8.

Competing interests: The authors declare no competing interests.

Reprints and permission information is available online at http://npg.nature.com/reprintsandpermissions/

Publisher's note: Springer Nature remains neutral with regard to jurisdictional claims in published maps and institutional affiliations.